ORIGINAL ARTICLE

A nonenzymatic laser-induced flexible amperometric graphene electrode for glucose detection in saliva

Betty Edem Nugba[1,2] · A. A. El-Moneim[2,3] · Nahla O. Mousa[4] · Ahmed Osman[1]

Abstract

Graphene is a suitable transducer for wearable sensors because of its high conductivity, large specific surface area, flexibility, and other unique considerable features. Using a simple, fast galvanic pulse electrodeposition approach, a unique nonenzymatic glucose amperometric electrode was successfully developed based on well-distributed fine Cu nanoparticles anchored on the surface of 3D structure laser-induced graphene. The fabricated electrode allows glucose detection with a sensitivity of 2665 µA/mM/cm^2, a response time of less than 5 s, a linear range of 0.03–4.5 mM, and a LOD of 0.023 µM. It also detects glucose selectively in the presence of interfering species such as ascorbic acid and urea. These provide the designed electrode the advantages for glucose sensing in saliva with 97% accuracy and present it among the best saliva-range non-enzymatic glucose sensors reported to date for real-life diagnostic applications.

1 Introduction

Since the discovery of biosensors, many materials, including graphene, have been proposed for sensing biofluids [1]. Graphene has received much interest recently due to its potential to

✉ Betty Edem Nugba
betty.nugba@ejust.edu.eg

A. A. El-Moneim
Ahmed.abdelmoneim@ejust.edu.eg

Nahla O. Mousa
Nahla.osama@ejust.edu.eg

Ahmed Osman
Ahmed.Osman@ejust.edu.eg

[1] Biotechnology Program, Institute of Basic and Applied Sciences, Egypt-Japan University of Science and Technology, Borg Al Arab City, P.O. Box 179, Alexandria, Egypt

[2] Graphene Center of Excellence for Energy and Electronics Applications, Egypt-Japan University of Science and Technology, Borg Al Arab City, P.O. Box 179, Alexandria, Egypt

[3] Nanoscience Program, Institute of Basic and Applied Sciences, Egypt-Japan University of Science and Technology, Borg Al Arab City, P.O. Box 179, Alexandria, Egypt

[4] Faculty of Science, Cairo University, Giza, Egypt

deliver high conductivity [2] and rate of heterogeneous electron transport [3, 4], excellent surface area, and other outstanding qualities [5]. Researchers suggested a number of processes for making graphene, including chemical methods, chemical or plasma exfoliation, and mechanical splitting from raw graphite [6]. Due to their high production costs, high energy consumption, low effectiveness, bulkiness, and chemical pollution, these technologies' industrial applicability is constrained [7].

Polyimide (PI) was discovered in 2014 as a possible substrate to be directly converted to Laser-Induced Graphene (LIG) using different types of pulsed laser irradiations [8–11]. Without requiring high-temperature procedures, solvents, or subsequent treatment, the pulsed laser irradiation process photothermally transforms carbon atoms from dense sp^3 structure to highly conductive 3D porous sp^2 of LIG electrodes or devices in one shot [12]. LIG has been proposed as an excellent transducer or sensing material in various sensing applications, including humidity, gas, strain, temperature, pressure, and biofluids sensing [4, 11, 13–20]. Biosensing, the focus of this study, typically refers to detecting molecules or biomolecules using a device employing a biological component [21].

Biosensors have been applied in many fields that involve the sensing of enzymes [22, 23], direct detection of pathogens [24–27], as well as infectious and non-infectious diseases like the detection of glucose in diabetes [28–33].

Glucose-detecting biosensors are usually either enzymatic or non-enzymatic biosensors. The enzymatic biosensors detect glucose by using glucose oxidase as the detecting agent [34], while non-enzymatic biosensors use metals capable of selectively detecting glucose. These metals are either transition and noble metals or metal oxides that have been proven to detect glucose in a pool of other biochemically reactive compounds. Some of these metals include Cu, Ni, Au, Pd, Co, Mg or a combination of any of these metals [1–6]. These metals chemically react with glucose to produce gluconic acid, a compound that is chemically detected. The delicate and expensive nature of enzymatic glucose biosensors has led to the design of non-enzymatic biosensors. They are popular because they have high catalytic activity, are low-cost and environmentally friendly, are fast in detecting glucose, and do not require special storage conditions. Since Copper nanoparticles (Cu NPs) have excellent catalytic properties and work well with other nanostructures such as carbon nanotubes (CNT) and graphene, they are frequently utilized as a modified electrode in glucose sensors [35–38]. Different deposition methods like drop casting, growth, electroless deposition [7] and direct electrodeposition [8].

Recently pulse plating proved to be an efficient means of depositing a metallic film with controlled porosity and particle size and electrical resistivity [39]. Optimizing these features is generally needed for enhancing the catalytic activity and sensing performance of active Cu NPs. Accordingly, we report in the present study about utilizing a galvanic pulse electrodeposition approach for the deposition of Cu NPs on LIG to enhance its sensing performance for glucose.

Sweat and saliva glucose concentrations are reliable indicators of a patient's blood glucose levels. [36]. There has been a rise in the development of saliva-based glucose sensing over the past years but still without convenience. The use of microchips and microfluidic devices for Point of Care (POC) detection of salivary glucose levels has significantly replaced optical measuring techniques, which need laborious pre-processing using expensive reagents and sophisticated equipment. A few examples are the non-enzymatic glucose biosensors [40], the paper strip-based pH indicator and glucose sensor [40], and a mouthguard glucose biosensor [41]. A flaw related to reduced glucose levels in saliva still exists despite all of these advancements. Therefore, to adapt and enhance the current salivary sensors for continuous monitoring of glucose, researchers must increase the performance of the sensors in terms of detecting technology, device structure, sensitivity, detection limit, and selectivity, among other variables. This paper focuses on developing a nonenzymatic glucose sensor capable of detecting glucose in saliva.

In this study, a CO_2 laser is used to induce graphene fibers on a flexible polyimide substrate to give a 3D conductive platform of LIG electrode for the pulse plating of Cu NPs. For the first time, this method produced very sensitive glucose electrode strips that could easily detect low glucose levels in human saliva.

2 Materials and methods

2.1 Materials

Ultrapure laboratory-grade deionized water was used to prepare all solutions. Potassium hexacyanoferrate III ($K_3[Fe (CN)_6]$), potassium hexacyanoferrate III ($K_4[Fe (CN)_6]\cdot 3H_2O$, Potassium chloride (KCl), Sodium hydroxide (NaOH), copper sulfate, anhydrous($CuSO_4$), absolute ethanol, and sodium sulfate (Na_2SO_4) were obtained from Thermo Fischer Scientific. Polyimide film of 125 μ m thickness was obtained from Sigma Aldrich.

2.2 LIG Design and fabrication

A computer-assisted CO_2 laser machine (VLS 3.50, Universal laser systems, Inc. VLS3.5) was used for engraving graphene on polyimide (PI) substrate to form conductive LIG working electrodes. The LIG was engraved in the Rast mode and cut out with the Vect mode of the machine. The laser machine's power and speed were adjusted at 1000 PPI (pulses per inch) to generate LIG with the lowest average resistivity, affecting the electrodes' charge transfer and their sensitivity to biofluids. The electrode is engraved by the laser machine in about two minutes (Fig. 1).

2.3 Pulsed current deposition of Cu NPs on LIG

The working area of LIG electrode was modified with copper nanoparticles (Cu NPs) using the pulsed current deposition (PCD) technique. The plating process was conducted in magnetically stirred $CuSO_4$ (5 mM) and Na_2SO_4 (50 mM) electrolytes at room temperature using three electrodes.

2.4 Morphological and structural characterizations

The morphological features of LIG and modified Cu NPs/ LIG electrodes were characterized using Scanning Electron Microscopy (SEM) (JEOL JSM-6010LV) and Transmission Electron Microscopy. (TEM) (JEOL JEM-2010F) complemented with electron dispersive spectroscopy (EDS) (JEOL JEM-2010F). The structural properties and bonding configurations of the electrodes were characterized using; XRD (Shimadzu, XRD-6100), FTIR (Bruker, VERTEX 70v), Raman (Bruker, Senterra II) Raman microscope, and XPS K-ALPHA (ThermoFisher Scientific, USA) characterization techniques. The films' electrical conductivity σ (Sm^{-1}) was measured using a Four Point probe configuration using an Oscilla Built-in Measurement device. Glucose concentration
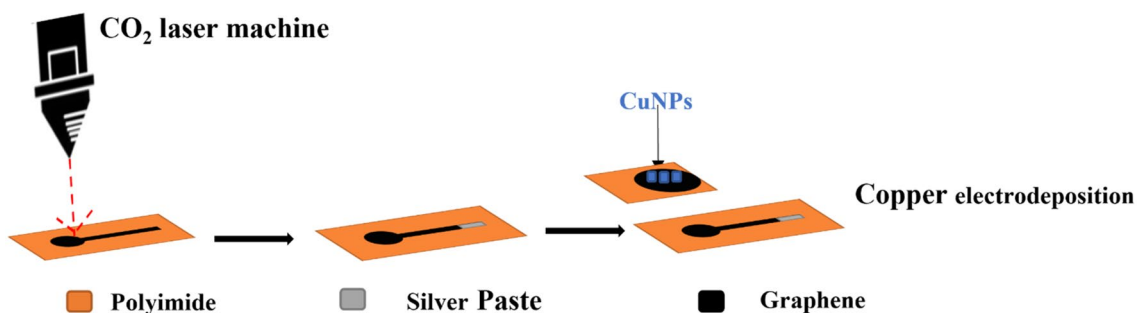
Fig. 1 Fabrication process of the Cu/LIG electrode

measurements were performed with a UV–Vis-NIR spectrophotometer (Shimadzu Scientific Instruments).

2.5 Electrochemical characterization

Using a Versa-STAT4 potentiostat and a three-electrode system, cyclic voltammetry (CV) and electrochemical impedance spectroscopy (EIS) measurements were carried out to evaluate the catalytic activity of the manufactured electrodes. The LIG-based films, which were designed using CorelDraw to have a circular shape (diameter = 5 mm), Ag/AgCl, and platinum wire, were used as working, reference, and counter electrodes, respectively.

To determine the ideal pulsing parameters that produce an electrode with the highest catalytic activity or peak current, EIS experiments at a frequency range of 100 kHz-0.1 Hz and cyclic voltammetry within a potential window of -0.4 V$-+0.6$ V(Ag/AgCl) at a scan rate of 100 mVs^{-1} were conducted in 2 mM K$_3$[Fe (CN)$_6$]+2 mM K$_4$[Fe(CN)$_6$] in 0.1 M KCl electrolyte. Nyquist plots were used to plot the EIS and fit it to the comparable Randles circuit.

Cyclic voltammetry tests were carried out for glucose detection and selectivity measurements in 0.1 M NaOH solution in the presence and absence of glucose additions. At room temperature, steady stirring was used to conduct the chronoamperometry and CV tests. Consecutive additions of concentrated glucose solution were introduced using a pipette with a droplet size of about 25 µl/drop.

2.6 Glucose sensing in serum and saliva

Following all ethical protocols, whole blood and saliva samples were collected from three consented male subjects to be tested with the modified biosensor. A commercial glucose sensing kit (Bioscien ARENA glucose testing kit) was used to test for glucose in plasma samples collected from the three male subjects. Glucose concentration was detected by an endpoint colorimetric method using a UV–Vis spectrophotometer at 546 nm. The absorbance was read, and the concentration was calculated by comparing it to a standard. The

CuNPs/LIG biosensor was used to test for glucose in saliva by adding a volume of saliva to 0.1 M NaOH solution. The current was noted, and the concentration was determined. We compared the results obtained from testing saliva with our modified electrodes to those obtained from the commercial kit, which serves as a reference.

3 Results and discussion

3.1 Lasing of PI

It is widely known that when PI film is exposed to high-intensity laser radiation, such as CO2 laser, the PI depolymerizes, resulting in carbonization and graphitization [9]. The development of gases produced during oxidation, the production of a porous structure, and broken and recombined C=O and N≡C bonds in polyimide all contribute to the final formation of the black graphitic result. Differences in the morphology and conductivity of the LIG produced under various laser parameters, such as laser power, speed, pulses per inch, image density, and defocus distance, are caused by the generation and the pace at which gas is released throughout the gasification process.

While maintaining other operating parameters (such as image density of 5 and defocus distance of 0 mm) unchanged, the processing-structure-conductivity relationship of the LIG is systematically investigated in the present study using a Four Probe analysis with laser power in the range of 2–8% W and speed in the range of 3–9 cms^{-1}.). In general, it was observed that increasing the power up to a threshold value of 7% W increases the conductivity and thickness of the engraved film. The PI substrate begins to burn at a power higher than 7% W, and conductance is lowered. Meanwhile, a power of 2% W or lower resulted in no engravement of graphene at the PI substrate. On the other hand, a breakneck laser speed decreased the conductance significantly, while a very low laser speed-length the graphene engravement process. A simultaneous application of power at 7% W and speed of 4 cms^{-1} gave an optimized/

lowest sheet resistance of 28.8 Ωsq^{-1} This value is in the range of previously reported resistivity of 5–115 Ωsq^{-1} obtained after lasing of PI by others [9] and affirms the reduced defective rate of the graphitic tracks and/or oxidation of the manufactured LIG, more effective electrochemical active area and high rate of heterogeneous electron transfer. Accordingly, it can, therefore, be said that LIG is an excellent material for constructing high-performance analytical devices.

3.2 Morphology and structure characterization of LIG

The morphology and structure of pristine LIG at optimized lasing conditions were conducted using SEM, TEM, XRD, FTIR, and Raman characterization tools, as seen in Fig. 2.

The SEM image of LIG, Fig. 2a, reveals a 3D porous fibers network of a highly accessible surface area. In the high magnification TEM image, Fig. 2b, the graphene nanofibers surface plainly shows a lot of edges that confirm its graphitic and multilayer structure.

Figure 2c presents the XRD pattern of the LIG film. The pattern shows a major diffuse diffraction peak observed at $2\theta = 26.12°$, typical of the (002) graphene plane degree of graphitization. Another peak overlapped with the significant peak and centered at $2\theta = 22.7°$ corresponds to reduced GO. The minor peaks that appeared at $2\theta = 15.5°$ and $42°$ are also referred to as GO, confirming the incomplete conversion of the sp^3 carbons to sp^2 carbons even at the proposed optimized condition. However, the operating lasing parameters were ideal for having a film with the highest electrical conductivity.

The recorded FTIR spectrum of LIG powder, Fig. 2d, displays vibrational peaks typical of LIG structure, with the peaks seen at 3444, 2923, 1636, and 1384–1115 cm^{-1} indicating, respectively, the existence of hydroxyl group (O–H), sp^3 C–H bonds, C=O carbonyl group stretch, and C-O bonds [9]. Due to the transformation of the sp^3 carbons into sp^2 carbons, a lower sp^3 C–H peak was seen at 2850 cm^{-1} [10].

Figure 2e depicts the Raman spectrum of LIG, which exhibits three distinctive peaks: the D peak at 1340 cm^{-1}, which indicates structural disorder in the sp^2 carbon lattice (for example, as a result of the covalently bonded oxygen characteristic of LIG) [12], a strong first-order G peak at 1580 cm^{-1}, which originated from graphitic carbon, and a 2D peak at 2708 cm^{-1}, which is caused by second-order zone The I_D/I_G and I_{2D}/I_G intensity ratios exhibit values of 0.85 and 1.7, respectively, showing the faulty and multilayer character of graphene sheets.

In brief, the LIG displays a 3D porous structure with high conductivity that potentially could provide a versatile platform for supporting the deposition of CuNPs and building

highly sensitive non-enzymatic glucose sensing devices, as seen in the upcoming session.

3.3 LIG modification by CuNPs using pulse current deposition (PCD)

In PCD, the current is applied in modulated waves, where three parameters can be varied independently; pulse current, pulse time, and off-pulse time. These variables determine the physical characteristics of the deposits obtained from the given electrolyte. Herein, we examined the influence of pulsing current and the number of the complete pulsing cycle (one complete cycle is off + on-time cycle) on the catalytic activities of the modified CuNPs-LIG electrodes, Fig. 3a and b, respectively, with a constant first current of 0.0002A. The catalytic activity of the modified electrodes is expressed, hereafter, as the recorded value of the peak current of cyclic voltammograms measured in an electrolyte containing 2 mM $K_3[Fe(CN)_6] + 2$ mM $K_4[Fe(CN)_6]$ in 0.1 M KCl. In Fig. 3a it can be seen that the increase in the pulse current from 0.25 to 2.0 mA at 350 pulsing cycles leads to an increase in the peak current till it approaches a constant value of 0.0009 A at a pulsing current of ≥ 1.0 mA, the second current. Meanwhile, the variation in the number of pulsing cycles, from 100 to 550 cycles, at an ideal pulse current of 0.0002 and 1.0 mA affects the catalytic activity of the modified electrodes, as depicted in Fig. 3c. The modified Cu NPs/LIG electrode obtained after 350 plating cycles exhibits the highest peak current among the examined electrodes. In brief, Cu NPs, as an electrode modifier, anchoring LIG with the highest catalytic activity is obtained at optimized/ideal pulse deposition conditions of 350 plating cycles at a pulse current of 0.0002A and 1.0 mA. The morphological and structural features of this electrode are given in detail in Fig. 3.

The morphological, structural, and composition characteristics of modified CuNPs-LIG electrode was examined using TEM/EDS and XPS characterization techniques.

The surface of the 3D porous fibrous network of LIG has been coated with well-dispersed Cu NPs (in red color) with an average particle size of 20 nm, Fig. 4a. According to the elemental analysis via/EDS, Fig. 4b, the CuNPs-LIG composite shows a composition of 17 wt% copper, 2 wt% oxygen, and the remainder of carbon and nitrogen. The significant concentration of CuNPs reveals the depositing bath's strong throwing ability under the prevailing pulse deposition conditions.

XPS study further supports the loading of CuNPs on LIG. The broad spectrum of the XPS measurement is shown in Fig. 4c, with a strong C 1 s peak at 285.5 eV and two smaller peaks of N 1 s at 400.00 eV (with 3.3% nitrogen mass concentration) and O 1 s at 533.26 eV. (with 5.2% oxygen mass concentration). Because of their evaporation and release owing to the photothermal impact of the CO_2 laser, nitrogen
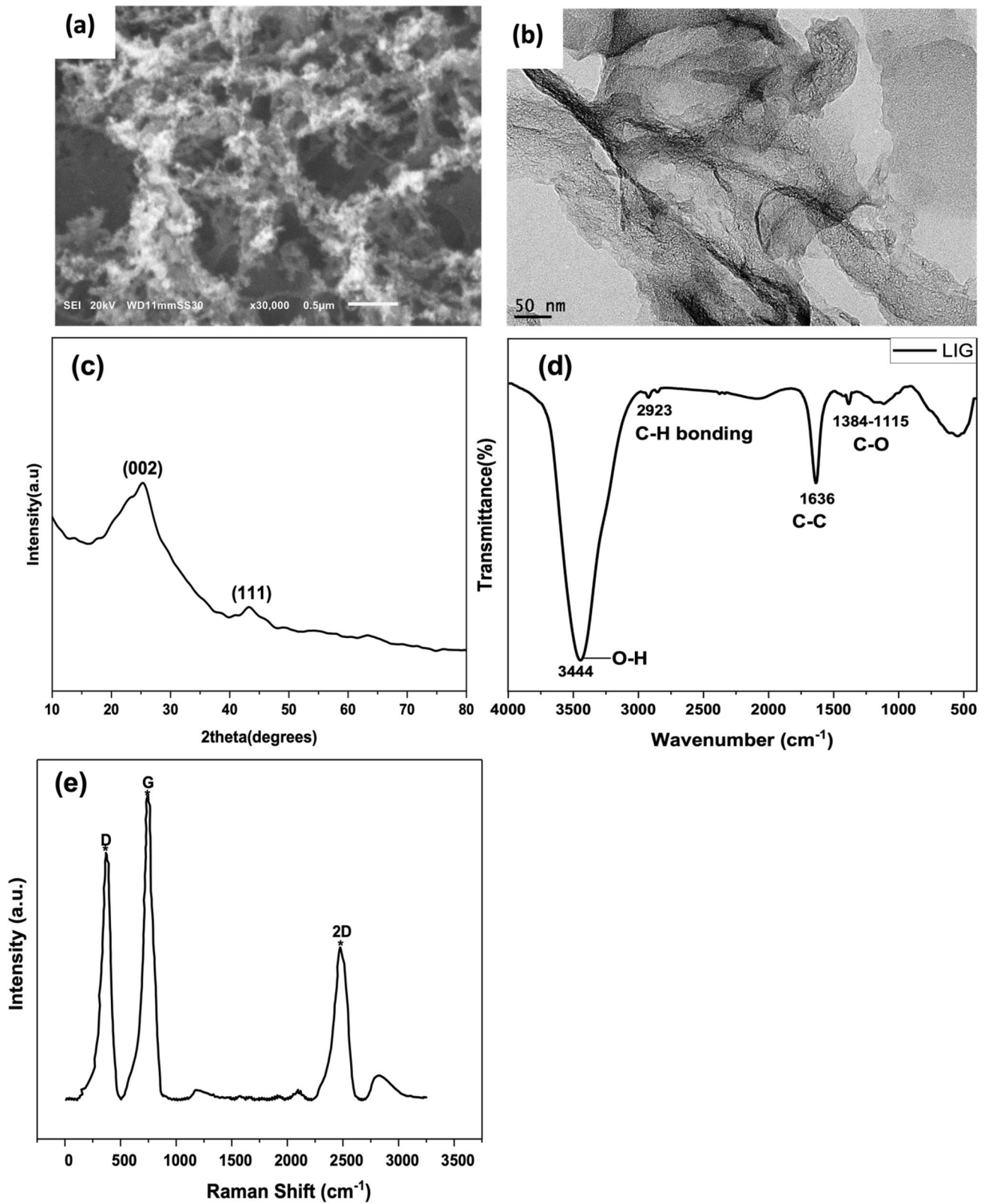
Fig. 2 **a** SEM and **b** TEM images, **c** XRD pattern, **d** FTIR, and **e** Raman spectra of pristine LIG
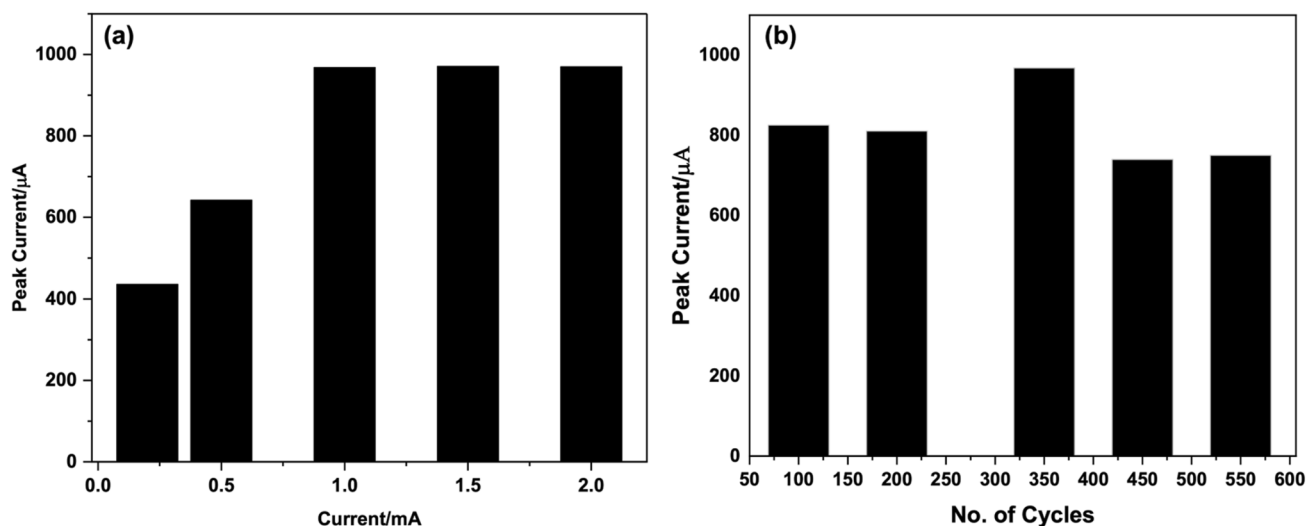
Fig. 3 Variation in the recorded value of peak current of cyclic voltammograms measured in an electrolyte containing 2 mM $K_3[Fe(CN)_6]$ and 2 mM $K_4[Fe(CN)_6]$ in 0.1 M KCl for modified CuNPs-LIG electrodes prepared by galvanic pulse deposition at different values of **a** pulse current and **b** pulse deposition cycles
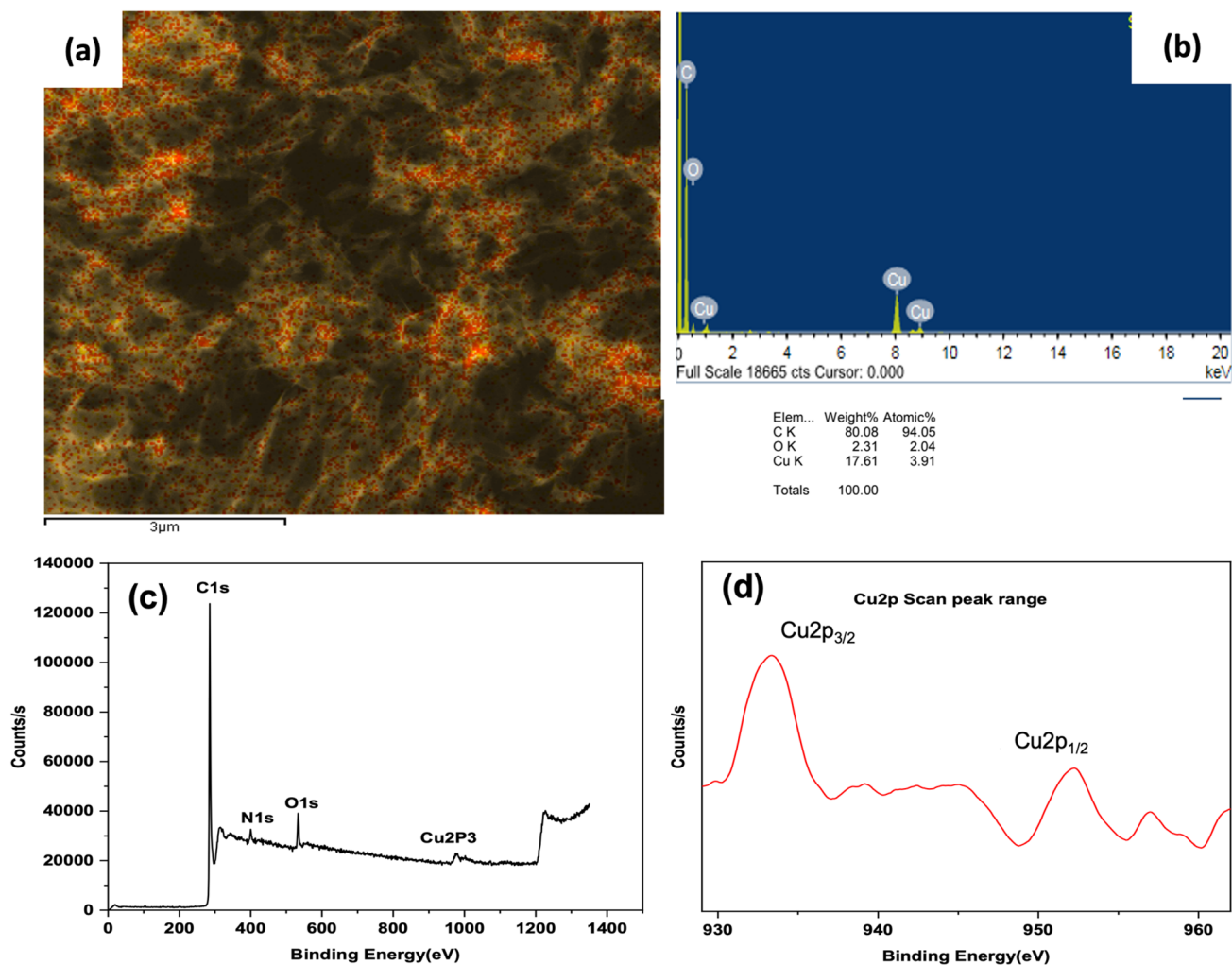

Fig. 4 **a** TEM image, **b** TEM/EDS analysis spectrum, **c** XPS wide spectrum and **d** XPS Cu 2p spectrum of modified CuNPs-LIG electrode

and oxygen are considerably less abundant on LIG than they are on the PI substrate, which suggests that LIG has undergone extensive graphitization. The peak location of Cu $2p_{3/2}$ is detected with a binding energy of 932.08 eV. (5% copper mass concentration), Fig. 4d. It would be necessary to place exact limitations on the BE, FWHM, and peak-shape parameters to quantify the predicted mixture of Cu(0), Cu(I), and Cu(II) species under the Cu $2p_{3/2}$ peak. Due to the overlap of these three components' extremely near-peak locations, the resolution of these components will be challenging. As a result, this study shows the initial deposition of metallic copper Cu(0) and a potential secondary deposition of copper oxides.

3.4 Electrochemical characterization of CuNPs-LIG electrode

The essential idea behind many electrochemical glucose sensors is that the kinetics of glucose oxidation produces a significant faradaic current [42]. This current correlates to the faradaic process, which typically comprises two stages. In the first phase, there is adsorption of glucose unto the surface of the active material, which causes redox reactions to occur, resulting in an electron transfer. In the next phase, there is an interfacial transport of electrons from the surface of the active material to the supporting material [43]. Therefore, increasing electron transport can considerably improve the faradaic process, accelerating glucose oxidation and improving the functionality of glucose sensors. By testing the EIS and CV behaviour of the LIG and Cu NPs-LIG electrodes in 2 mM $K_3[Fe (CN)_6]$ + 2 mM $K_4[Fe (CN)_6]$ in 0.1 M KCl electrolyte, the CuNPs-LIG interfacial electron transport was reported in detail.

The measured Nyquist plots for the LIG and CuNPs-LIG electrodes in the 100 kHz–100 MHz frequency range are shown in Fig. 5a. The Figures are made up of a low-frequency linear portion for the Warburg diffusion process typical of porous electrodes and a high-frequency area semi-circle. The computed charge transfer resistance of $R_{ct.} = 60$ and 15 Ω, for LIG and CuNPs-LIG electrodes, respectively, indicating a reduction in the impedance to charge transfer rate by the deposition of CuNPs on LIG, is obtained by fitting the Nyquist plots with the Randle circuit. In contrast, the modified CuNPs-LIG electrode has a steeper slope of the linear component in the low-frequency region than the LIG electrode, indicating more accessibility for ions via diffusion through the modified electrode surface.

Figure 5 shows a further correlation between the EIS results and those from cyclic voltammetry tests (b). The cathodic peak currents (i_{pc}) of the LIG and CuNPs-LIG are 768 and 968 μA, respectively, according to their CV curves. Further evidence is that the deposition of CuNPs on LIG increased the electron and ion transfer rate for the modified electrode having a greater enclosed integration area than that provided by LIG. In other words, loading LIG with CuNPs caused LIG's surface to experience greater interfacial electron transport.

3.5 Electrocatalytic oxidation of glucose

Figure 6a shows how the modified electrode's glucose oxidation is affected by scan rates (ν). The glucose oxidation peak's potentials undergo a positive shift when the scan rate is raised from 0.05 to 0.25 Vs^{-1}, while the peak current's values steadily rise. A strong correlation coefficient, R^2, of 0.998 is used to describe the linear change in the
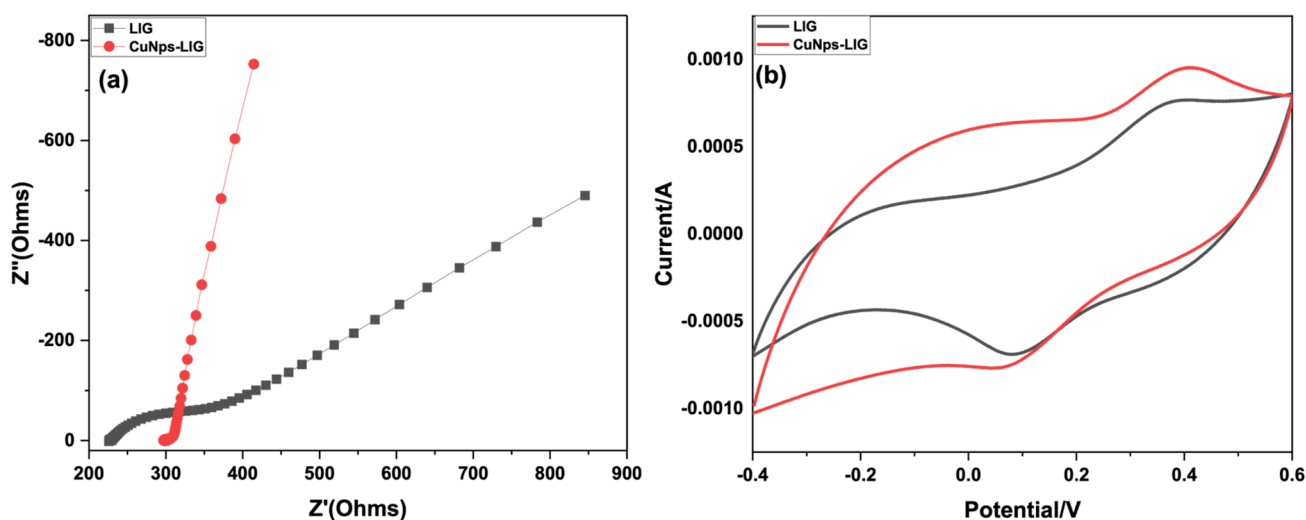

Fig. 5 **a** Nyquist plot and **b** CV curves of the CuNPs-LIG electrode in an electrolyte containing 2 mM $K_3[Fe(CN)_6]$ and 2 mM $K_4[Fe(CN)_6]$ in 0.1 M KCl
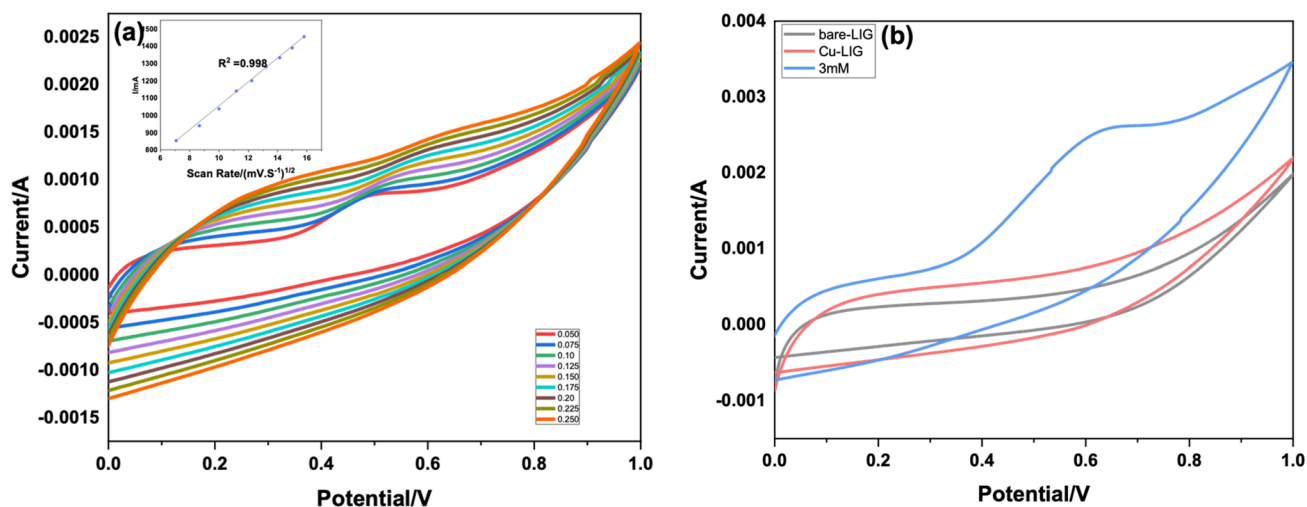
Fig. 6 **a** CV curves of LIG and CuNPs-LIG electrode in 0.1 M NaOH solution in the presence and absence of 3 mM glucose and **b** of CuNPs-LIG modified electrode in 0.1 M NaOH solution with 1 mM glucose at different scan rates ranging from 0.025 to 0.250 V-s^{-1}

present values of the oxidation peak with respect to $\nu^{1/2}$. This suggests the normal diffusion-controlled reaction of glucose oxidation at the modified electrode's surface and verifies the glucose's improved accessibility through the 3D porous structure of the modified conductive electrode [44].

With the use of CV measurements at 0.1 Vs^{-1} in a 0.1 M NaOH solution with and without the addition of 2 mM glucose, the activity of LIG and modified electrodes toward glucose oxidation were examined, Fig. 6b. In the absence of glucose, both electrodes do not even exhibit any redox peaks. Upon the addition of glucose, the modified electrode shows a considerable increase in current in an oxidation peak that appears at a potential of about 0.5 V, while none is seen with the LIG electrode, confirming that the CuNPs have a high electrocatalytic selectivity for the direct oxidation of glucose to gluconic acid [45].

3.6 Amperometric responses of the CuNPs-LIG electrode toward glucose oxidation

The activity of the electrodes toward glucose oxidation was further examined using the amperometry technique. To define the optimal potential for glucose oxidation using a fabricated modified electrode [46], the amperometric tests were conducted at potentials of 0.45, 0.5, 0.55 V, and 0.6 V with 0.45, 0.5, and 0.55 V represented in Fig. 7. This was done by titrating glucose solution to 0.1 M NaOH electrolyte in each step after every 10 s, Fig. 7. The maximum amperometric current was measured at 0.55 V, and hence this value is presented hereafter as an ideal sensing potential for additional amperometric studies on glucose oxidation.
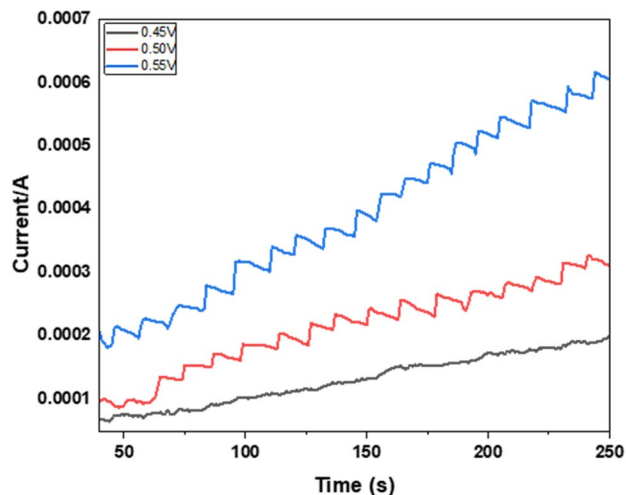

Fig. 7 Optimization of applied oxidation potentials using amperometric current response for CuNPs-LIG electrodes in 0.1 M NaOH with step titration of glucose

3.7 Detection of glucose in actual biological saliva samples

The amperometric response of the modified electrode was also examined after adding glucose drops of varying concentrations, in a detection range of 33 μM-1 mM, in 0.1 M NaOH solution, Fig. 8a. A step-shaped increase in the current response is recorded with an increase in the glucose concentration. The current-glucose concentration correlation was accordingly plotted, Fig. 8b, where it shows a linear range of 0.03–4.5 mM with R^2 of 0.99357, the sensitivity of 2665 mA/mM.cm^2 and LOD of 0.023 μM as the sensitivity, LOD and response in < 5 s.

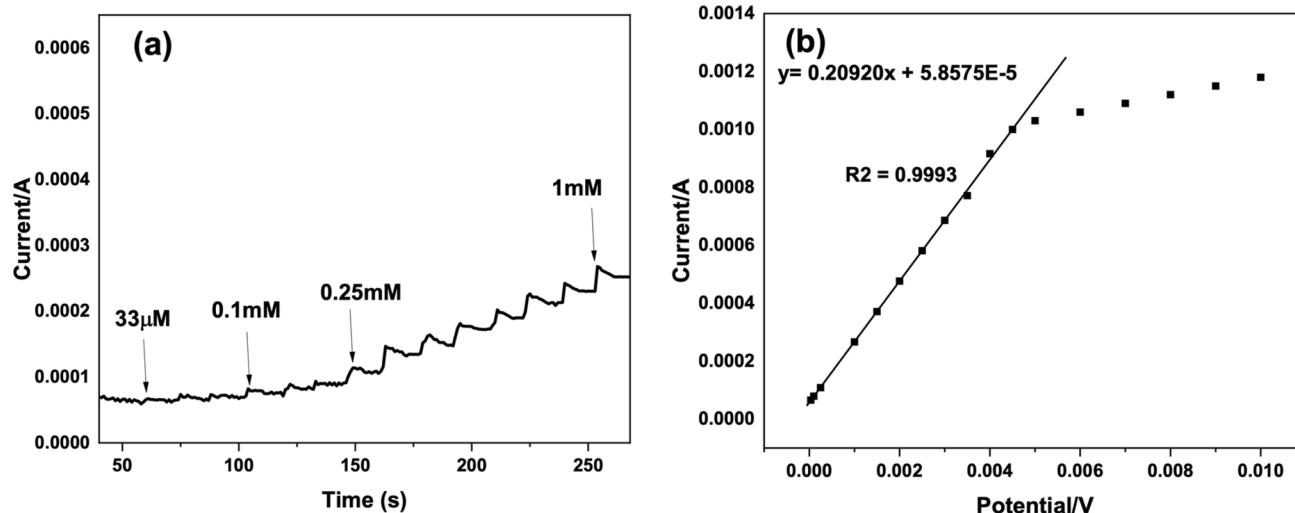**Fig. 8** **a** CuNPs-LIG electrodes' I-t response at 0.55 V in presence of different glucose concentrations in 0.1 M NaOH solution **b** the relationship between the current reaction and glucose level

Practically several interfering species, such as uric acid (UA), ascorbic acid (AA), and urea, are present with glucose in the genuine blood samples and their concentrations are considerably lower than that of glucose in actual serum. These organisms' are well-known with quick electron transfer rates that could cause interference with glucose monitoring. Therefore, it would appear crucial to assess the changed sensor's selectivity in the presence of these interfering species. The interference experiment was carried out using the amperometric test at 0.55 V by adding 1.0 mM glucose and 0.1 mM of urea, AA, and NaCl solutions to 0.1 mM NaOH electrolyte, Figure. No significant signal change upon adding any of these species, indicating the high selectivity of the modified electrode towards the direct oxidation of glucose (Fig. 9).

3.8 Detection of glucose in actual biological saliva samples

For real-life application, saliva glucose concentration in samples taken from three male subjects was detected via CuNPs-LIG electrode using an amperometric measurement technique. The obtained results were compared with the detected glucose concentration in plasma samples taken from the same subjects using a commercial spectrophotometer detection-based enzymatic glucose test kit. The formula [plasma glucose (mg/dL)] = 95.607 + 27.710 [saliva glucose (mg/dL)] was used to convert between the plasma glucose concentration and saliva glucose concentration [36]. The measured random blood glucose for subjects 1, 2, and 3 with their corresponding derived saliva glucose concentrations are presented in Table 1 and compared with the saliva glucose concentrations of the three subjects measured by
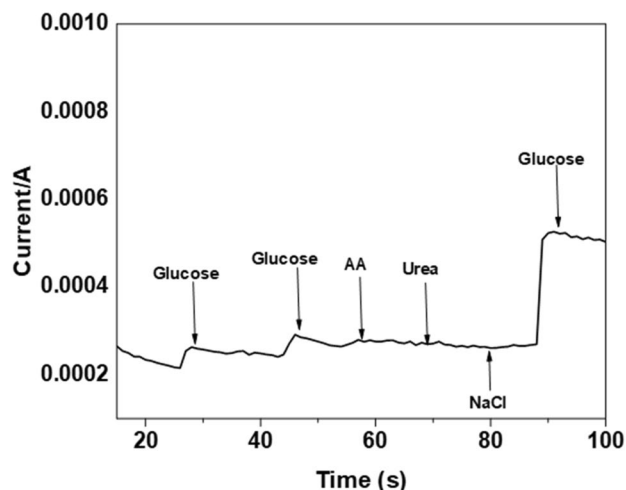

Fig. 9 I-t curves of CuNPs-LIG sensor at 0.55 V after sequential addition of 1.0 mM glucose, 0.1 mM ascorbic acid, and 0.1 mM urea to 0.1 M NaOH solution

CuNPs-LIG electrode. The results obtained after saliva glucose measurements were in very close agreement with those obtained from their corresponding blood glucose measurements by about 97%. This demonstrates the reliability of our modified electrode for actual biological samples and realistic glucose detection.

According to the analysis of the glucose electro-oxidation reaction (GER) results on the designed Cu NPs/LIG sensor prototype, the route of mass and charge transport between Cu and Cu^{2+} species appears to influence the glucose sensing properties expressed in terms of sensitivity, detection limit, and linear detection limit [47]. According to earlier findings, Cu/CuO spontaneously oxidizes in a NaOH electrolyte to

Table 1 Comparison of saliva glucose concentration obtained using the designed Cu NPs-LIG electrode with the results of blood glucose concentration measured using a commercial spectrophotometer for three male subjects

	Blood glucose (mg/dl)	Saliva glucose conc (mg/dl) mathmetically estimated from the measured blood glucose conc	CuNPs-LIG Saliva glucose conc (mg/dl)	Difference %
Subject 1	144	1.21	1.18	2.5
Subject 2	116	0.92	0.90	2.3
Subject 3	96	0.71	0.69	1.0

yield $Cu(OH)_2$, which then electrochemically reacts with the OH^- species to produce $CuOOH$, which drives the development of the GER process as detailed below [48];

$$Cu + 2OH^- \rightarrow CuO + H_2O + 2e^- \tag{1}$$

$$CuO + OH^- \rightarrow CuOOH \text{ or } CuO + H_2O + 2OH^- \rightarrow Cu(OH)_4^- + e^- \tag{2}$$

$$Cu(III) + \text{glucose} \rightarrow \text{gluconol actone} + Cu(II) \text{ Gluconolactone} \rightarrow \text{gluconic acid} \tag{3}$$
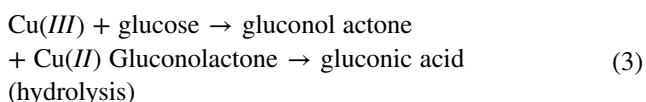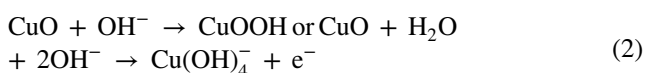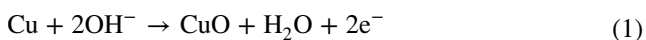(hydrolysis)

Table 2 compares the glucose sensing capabilities of our modified CuNPs-LIG electrode with those of existing non-enzymatic electrochemical glucose sensors based on Cu or Cu-their composites [49]. As a base for comparison, the flexible polyimide substrate's cheap cost and suggested production technique for our modified electrode are some of the key benefits of its utilization in biosensing applications when compared to the other expensive substrates that were used in the formulation of the biosensors by others, like glassy carbon substrate and silicon dioxide [50]. We also chose fast galvanic pulse electrodeposition for fine loading and well distribution CuNPs on LIG surface due to its effectiveness, ease of performing, and the deposition of well-dispersed

CuNPs on the 3D porous structure of electrochemically robust conductive LIG substrate. Human plasma/saliva was also tested to determine the ability of our modified electrode to select and test glucose in real-life applications in the presence of all the interfering species. These reasons give our electrode advantages over the other electrodes used in glucose biosensing displayed in Table 2, which reveals a higher catalytic activity, outstanding sensitivity, a comparably high linear range, and low detection limit of glucose sensing.

3.9 Flexibility and wettability of the electrode

The flexibility of the Cu NPs-LIG electrode was explored via examining the effect of bending angle and cycle on the electrode resistivity using a homemade test rig, Fig. 10a. As shown in Fig. 10b and c, the varying bending angle and cycle tests did not significantly affect the surface resistance of the electrode, leaving the electrode intact and referring to its robustness.

The traditional method for measuring a solid's wettability is the contact angle (θ) between a solid surface and a liquid droplet [51]. The wettability of carbon materials, including carbon fibers, carbon black, and carbon nanotubes, which are often more hydrophobic than metals [52], is highly influenced by their structural makeup and the

Table 2 Comparison of the glucose sensing performance of our modified CuNPs-LIG and other previously reported nonenzymatic electrochemical glucose electrodes

| Electrode materials	Response time	Potential (V)	Detection limit (μM)	Linear range (mM)	Real time sample	Sensitivity	Reference
GC/CoNSs/CHIT-RGO	N/A	0.45 (vs. SCE)	10	0.015	No	1921	[41]
GC/Cu Nanocubes/ Graphene	N/A	0.55 (vs. Ag/AgCl)	1	Up to 7.5	No	1096	[55]
CuNCs-DLEG	< 3	0.55 (vs. Ag/AgCl)	0.25	0.025–4.5	No	4532	[45]
GC/Cu NPs/Graphene	< 2	0.50 (vs. Ag/AgCl)	0.50	Up to 4.5	Serum	N/A	[18]
SPE /Pt-Cu^o/rGO	N/A	0.60 (vs. Ag/AgCl)	0.01	0.0005–12	No	3577	[56]
SiSiO$_2$/Ti/Pt/GNP/ PEDOT-GOx	N/A	N/A	0.03	0.01–50	No	≈14	[57, 58]
Au/Ni/LIG	< 1 s	0.55 (vs. Ag/AgCl)	1.5	0–4	Sweat, cell culture media	1200	[59]
Cu NPs-LIG	< 5 s	0.55 (vs. Ag/AgCl)	0.023	0.033–4.5	Plasma, saliva	2665	This work
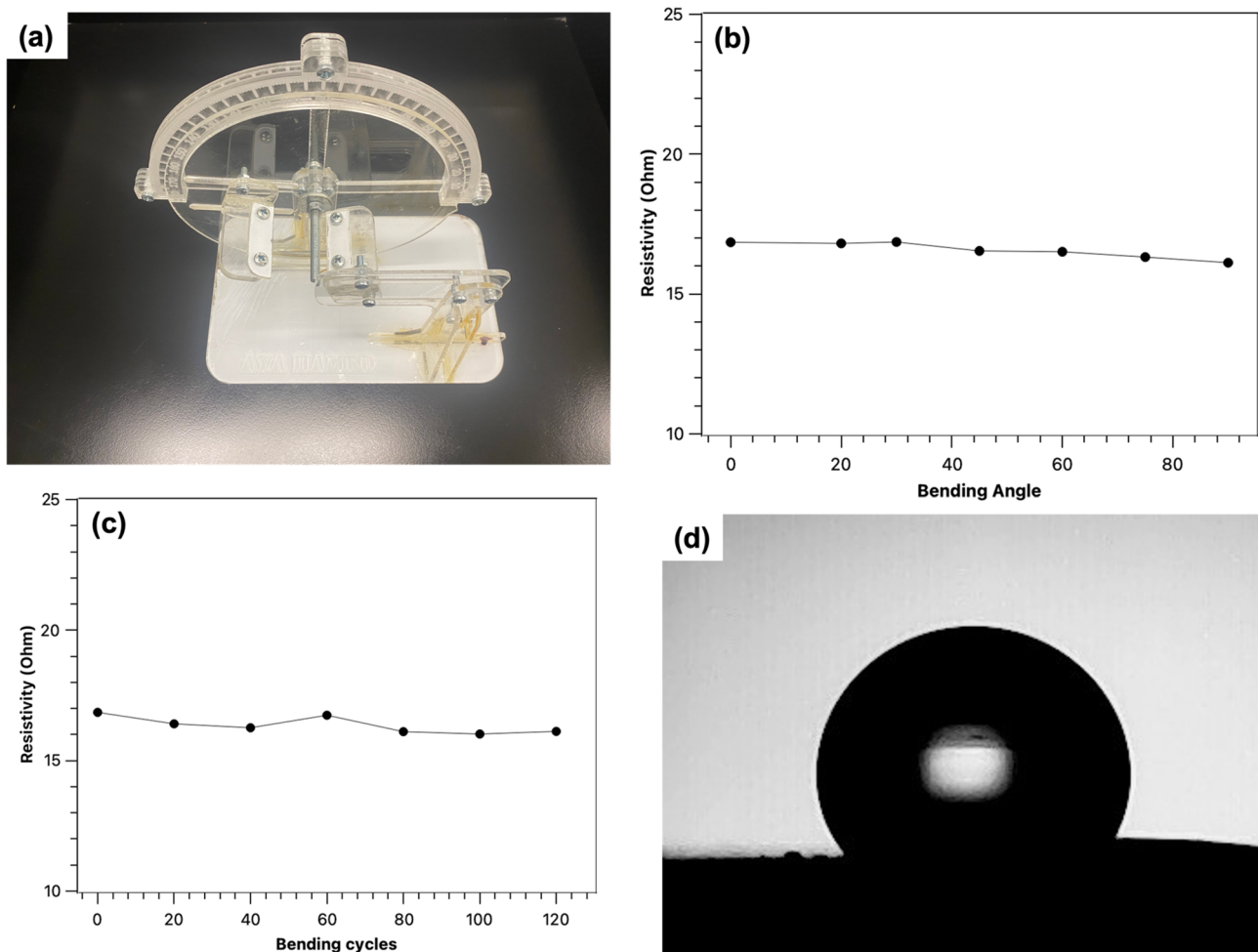
Fig. 10 **a** Homemade bending device, **b** Resistivity change of the Cu NPs-LIG electrode with bending angle **c** Resistivity change of the Cu NPs-LIG electrode with bending cycle at angle 75°, and **d** Wettability of Cu NPs-LIG electrode with water

heterogeneous atoms that make up the carbon surface [53]. Due to the absence of high-energy flaws near their surface, graphene is more hydrophobic. In addition, LIG has been widely reported in literature as a hydrophobic material. Graphene with hydrophobic properties can reduce liquid deposition and prevent contamination during the fabrication of electronic devices, which in this case, will improve metal deposition from the electrolyte [54]. Investigations into the effect electrodeposited Cu NPs have on the wettability of LIG were initiated. As displayed in Fig. 10d, the hydrophobicity of LIG was unaffected, with a contact angle of 123 ° with the addition of Cu NPs. The hydrophobic nature of the electrode improves the deposition of the metal from the electrolyte unto the electrode.

The Cu NPs-LIG sensor was examined for the life stability test, where the biosensor was stored in an ambient environment and tested against 1 mM glucose concentration every 7 days for 35 days with sensitivity plotted against the number of days in Fig. 11. The biosensor remained over 94% of the initial response, which first shows the repeatability of the electrode after several days of use and the durability of the electrode.

4 Conclusion

This project illustrates the usage of engraved porous graphene (LIG) on a polyimide substrate and subsequent PCD of CuNPs of less than 29 nm in size for nonenzymatic glucose detection. The electrode can detect glucose in a linear range of 0.03–4.5 mM and LOD of 0.023 μM, which agrees favorably with literature reports. The high selectivity and sensitivity of the electrode, 2665 μA/mM/cm^2, gives it great potential for sensing low glucose concentration in saliva. The saliva glucose measurements taken with our modified electrode were evidently in very close agreement,
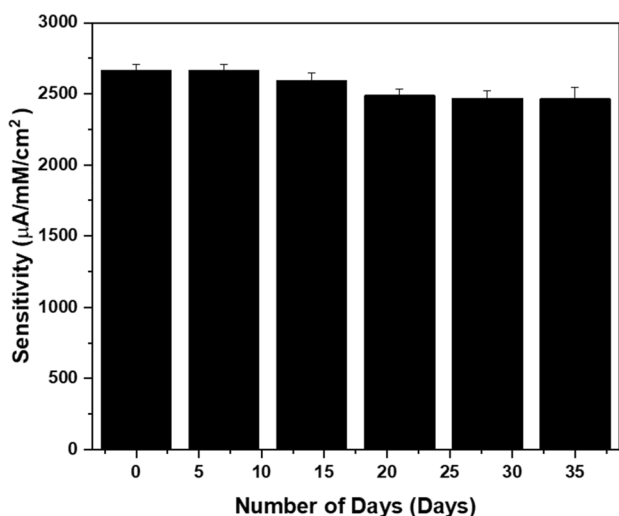
Fig. 11 Life stability of the sensor over a 35 days period

about 97%, with the saliva glucose measurements obtained from their corresponding blood glucose measurements. This shows the strong ability of our electrode to sense and measure glucose in a biological sample accurately.

Data availability The data that support these findings are within the article.

Declarations

Conflict of interest The authors of this manuscript declare no conflict of interest.

References

1. Suvarnaphaet P, Pechprasarn S (2017) Graphene-based materials for biosensors: a review. Sensors (Switzerland). 17:10. https://doi.org/10.3390/s17102161

2. Kuilla T, Bhadra S, Yao D, Kim NH, Bose S, Lee JH (2010) Recent advances in graphene based polymer composites. Prog Poly Sci (Oxford). 35:11. https://doi.org/10.1016/j.progpolymsci.2010.07.005

3. Pumera M (2011) Graphene in biosensing. Mater Today 14(7–8):308–315. https://doi.org/10.1016/S1369-7021(11)70160-2

4. Cui Y, Kundalwal SI, Kumar S (2016) Gas barrier performance of graphene/polymer nanocomposites. Carbon 98:313–333. https://doi.org/10.1016/j.carbon.2015.11.018

5. Smith AT, LaChance AM, Zeng S, Liu B, Sun L (2019) Synthesis, properties, and applications of graphene oxide/reduced graphene oxide and their nanocomposites. Nano Mater Sci 1(1):31–47. https://doi.org/10.1016/j.nanoms.2019.02.004

6. Han T et al (2019) Multifunctional flexible sensor based on laser-induced graphene. Sensors (Switzerland). 19(16):3477. https://doi.org/10.3390/s19163477

7. Wang L, Wang Z, Bakhtiyari AN, Zheng H (2020) A comparative study of laser-induced graphene by co_2 infrared laser and 355 nm ultraviolet (Uv) laser. Micromachines (Basel) 11(12):1–9. https://doi.org/10.3390/mi11121094

8. Lin J et al (2014) Laser-induced porous graphene films from commercial polymers. Nat Commun. https://doi.org/10.1038/ncomms6714

9. Huang L, Su J, Song Y, Ye R (2020) Laser-induced graphene: en route to smart sensing. Nano-Micro Lett. https://doi.org/10.1007/s40820-020-00496-0

10. Zhang Z, Song M, Hao J, Wu K, Li C, Hu C (2018) Visible light laser-induced graphene from phenolic resin: a new approach for directly writing graphene-based electrochemical devices on various substrates. Carbon N Y 127:287–296. https://doi.org/10.1016/j.carbon.2017.11.014

11. Carvalho AF et al (2018) Laser-induced graphene strain sensors produced by ultraviolet irradiation of polyimide. Advanc Function Mater. 28(52):1805271. https://doi.org/10.1002/adfm.201805271

12. Settu K, Chiu PT, Huang YM (2021) Laser-induced graphene-based enzymatic biosensor for glucose detection. Polymers (Basel). 13(16):2795. https://doi.org/10.3390/polym13162795

13. Mahmood F, Mahmood F, Zhang H, Lin J, Wan C (2020) Laser-induced graphene derived from kraft lignin for flexible supercapacitors. ACS Omega 5(24):14611–14618. https://doi.org/10.1021/acsomega.0c01293

14. Shim HC, van Tran C, Hyun S, bin J (2021) In, "Three-dimensional laser-induced holey graphene and its dry release transfer onto Cu foil for high-rate energy storage in lithium-ion batteries." Appl Surf Sci 564:150416. https://doi.org/10.1016/j.apsusc.2021.150416

15. Kwong Hong Tsang D et al (2019) Chemically functionalised graphene FET biosensor for the label-free sensing of exosomes. Sci Rep. https://doi.org/10.1038/s41598-019-50412-9

16. Cui T et al (2021) Ultrasensitive detection of covid-19 causative virus (Sars-cov-2) spike protein using laser induced graphene field-effect transistor. Molecules 26(22):6947. https://doi.org/10.3390/molecules26226947

17. Phetsang S, Kidkhunthod P, Chanlek N, Jakmunee J, Mungkornasawakul P, Ounnunkad K (2021) Copper/reduced graphene oxide film modified electrode for non-enzymatic glucose sensing application. Sci Rep. https://doi.org/10.1038/s41598-021-88747-x

18. Luo J, Jiang S, Zhang H, Jiang J, Liu X (2012) A novel non-enzymatic glucose sensor based on Cu nanoparticle modified graphene

sheets electrode. Anal Chim Acta 709:47–53. https://doi.org/10.1016/j.aca.2011.10.025

19. Jiang D et al (2014) Enhanced non-enzymatic glucose sensing based on copper nanoparticles decorated nitrogen-doped graphene. Biosens Bioelectron 54:273–278. https://doi.org/10.1016/j.bios.2013.11.005

20. Cardoso AR et al (2018) "Molecularly-imprinted chloramphenicol sensor with laser-induced graphene electrodes. Biosens Bioelectron 124:167–175

21. Mehrotra P (2016) Biosensors and their applications—a review. J Oral Biol Craniofac Res. 6(2):153–159. https://doi.org/10.1016/j.jobcr.2015.12.002

22. Venugopal V (2002) "Biosensors in fish production and quality control.". [Online]. Available: www.elsevier.com/locate/bios

23. Akyilmaz E, Yorganci E, Asav E (2010) Do copper ions activate tyrosinase enzyme? A biosensor model for the solution. Bioelectrochemistry 78(2):155–160. https://doi.org/10.1016/j.bioelechem.2009.09.007

24. Ercole C, del Gallo M, Mosiello L, Baccella S, Lepidi A (2003) Escherichia coli detection in vegetable food by a potentiometric biosensor. Sens Actuators B Chem 91(1–3):163–168. https://doi.org/10.1016/S0925-4005(03)00083-2

25. Torun Ö, Hakki Boyaci I, Temür E, Tamer U (2012) Comparison of sensing strategies in SPR biosensor for rapid and sensitive enumeration of bacteria. Biosens Bioelectron 37(1):53–60. https://doi.org/10.1016/j.bios.2012.04.034

26. Arora P, Sindhu A, Dilbaghi N, Chaudhury A (2011) Biosensors as innovative tools for the detection of food borne pathogens. Biosens Bioelectron 28(1):1–12. https://doi.org/10.1016/j.bios.2011.06.002

27. Riedel T et al (2014) Diagnosis of Epstein-Barr virus infection in clinical serum samples by an SPR biosensor assay. Biosens Bioelectron 55:278–284. https://doi.org/10.1016/j.bios.2013.12.011

28. Singh M, Kathuroju PK, Jampana N (2009) Polypyrrole based amperometric glucose biosensors. Sens Actu B Chem. 143(1):430–443. https://doi.org/10.1016/j.snb.2009.09.005

29. Newman JD, Turner APF (2005) "Home Blood Glucose Biosensors: A Commercial Perspective." [Online]. Available: www.Silsoe.cranfield.ac.uk

30. Wang J (2008) Electrochemical glucose biosensors. Chem Rev 108(2):814–825. https://doi.org/10.1021/cr068123a

31. Yoo EH, Lee SY (2010) Glucose biosensors: an overview of use in clinical practice. Sensors 10(5):4558–4576. https://doi.org/10.3390/s100504558

32. Wang J (2002) Glucose biosensors: 40 years of advances and challenges. Sens Update. 10(1):107–119

33. Ricci F et al (2005) Novel planar glucose biosensors for continuous monitoring use. Biosens Bioelectron 20(10):1993–2000. https://doi.org/10.1016/j.bios.2004.09.010

34. Study RB, Blunt BA, Barrett-Connor E, Wingard DL. 1991 "Evaluation of Fasting Plasma Glucose as Screening Test for N1DDM in Older Adults." [Online]. Available: http://diabetesjournals.org/care/article-pdf/14/11/989/440025/14-11-989.pdf

35. Daum KM, Hill RM (1982) Human tear glucose. Invest Ophthalmol Vis Sci 22(4):509–514

36. Panchbhai AS (2012) Correlation of salivary glucose level with blood glucose level in diabetes mellitus. J Oral Maxillofac Res. https://doi.org/10.5037/jomr.2012.3303

37. Yoon H et al (2020) A chemically modified laser-induced porous graphene based flexible and ultrasensitive electrochemical biosensor for sweat glucose detection. Sens Actu B Chem. https://doi.org/10.1016/j.snb.2020.127866

38. Kumar S, Padmashree S, Jayalekshmi R (2014) Correlation of salivary glucose, blood glucose and oral candidal carriage in the saliva of type 2 diabetics: a case-control study. Contemp Clin Dent 5(3):312–317. https://doi.org/10.4103/0976-237X.137925

39. German N, Ramanaviciene A, Ramanavicius A (2020) Formation and electrochemical evaluation of polyaniline and polypyrrole nanocomposites based on glucose oxidase and gold nanostructures. Polymers (Basel) 12(12):1–20. https://doi.org/10.3390/polym12123026

40. Soni A, Jha SK (2015) A paper strip based non-invasive glucose biosensor for salivary analysis. Bios Bioelect 67:763–768. https://doi.org/10.1016/j.bios.2014.09.042

41. Haghighi B, Karimi B, Tavahodi M, Behzadneia H (2015) Fabrication of a nonenzymatic glucose sensor using Pd-nanoparticles decorated ionic liquid derived fibrillated mesoporous carbon. Mater Sci Eng, C 52:219–224. https://doi.org/10.1016/j.msec.2015.03.045

42. Gamil M, Tabata O, Nakamura K, El-Bab AMRF, El-Moneim AA (2014) Investigation of a new high sensitive micro-electromechanical strain gauge sensor based on graphene piezoresistivity. Key Eng Mater 605:207–210. https://doi.org/10.4028/www.scientific.net/KEM.605.207

43. El-Moneim AA, Akiyama E, Ismail KM, Hashimoto K (2011) Corrosion behaviour of sputter-deposited Mg–Zr alloys in a borate buffer solution. Corros Sci 53(9):2988–2993. https://doi.org/10.1016/j.corsci.2011.05.043

44. Rashed AE, El-Moneim AA (2017) Two steps synthesis approach of MnO_2/graphene nanoplates/graphite composite electrode for supercapacitor application. Mater Today Energy 3:24–31. https://doi.org/10.1016/j.mtener.2017.02.004

45. Tehrani F, Bavarian B (2016) Facile and scalable disposable sensor based on laser engraved graphene for electrochemical detection of glucose. Sci Rep. https://doi.org/10.1038/srep27975

46. Shaker A, Hassanin AH, Shaalan NM, Hassan MA, El-Moneim AA (2019) Micropatterned flexible strain gauge sensor based on wet electrospun polyurethane/PEDOT: PSS nanofibers. Smart Mater Struct 28(7):075029

47. Das D, Kim DM, Park DS, Shim YB (2011) A glucose sensor based on an aminophenyl boronic acid bonded conducting polymer. Electroanalysis 23(9):2036–2041. https://doi.org/10.1002/elan.201100145

48. Arakawa T et al (2016) Mouthguard biosensor with telemetry system for monitoring of saliva glucose: a novel cavities sensor. Biosens Bioelectron 84:106–111. https://doi.org/10.1016/j.bios.2015.12.014

49. Qin L, He L, Zhao J, Zhao B, Yin Y, Yang Y (2017) Synthesis of Ni/Au multilayer nanowire arrays for ultrasensitive non-enzymatic sensing of glucose. Sens Actuators B Chem 240:779–784. https://doi.org/10.1016/j.snb.2016.09.041

50. El-Deen AG, Hussein El-Shafei M, Hessein A, Hassanin AH, Shaalan NM, El-Moneim AA (2020) High-performance asymmetric supercapacitor-based hierarchical $NiCo_2O_4$@ carbon nanofibers//Activated multichannel carbon nanofibers. Nanotechnology 31(36):365404

51. El-Khatib KM, Abou Helal MO, El-Moneim AA, Tawfik H (2004) Corrosion stability of SUS316L HVOF sprayed coatings as lightweight bipolar plate materials in PEM fuel cells. Anti-Corr Methods Mater. 51(2):136–142. https://doi.org/10.1108/00035590410523238

52. Fan Z et al (2013) A flexible and disposable hybrid electrode based on Cu nanowires modified graphene transparent electrode for non-enzymatic glucose sensor. Electrochim Acta 109:602–608. https://doi.org/10.1016/j.electacta.2013.07.153

53. Li M et al (2021) The role of electrode wettability in electrochemical reduction of carbon dioxide. J Mater Chem A Mater 9(35):19369–19409. https://doi.org/10.1039/D1TA03636J

54. Feng J, Guo Z (2019) Wettability of graphene: from influencing factors and reversible conversions to potential applications. Nanoscale Horiz 4(2):339–364. https://doi.org/10.1039/C8NH00348C

55. Yang J, de Zhang W, Gunasekaran S (2010) An amperometric non-enzymatic glucose sensor by electrodepositing copper nanocubes onto vertically well-aligned multi-walled carbon nanotube arrays. Biosens Bioelectron 26(1):279–284. https://doi.org/10.1016/j.bios.2010.06.014

56. Dharaa K, Stanley J, Ta T, Bipin GN, Babu STG (2014) Pt-CuO nanoparticles decorated reduced graphene oxide for the fabrication of highly sensitive non-enzymatic disposable glucose sensor. Sens Actuators B 195:197–205

57. Claussen JC et al (2012) Nanostructuring platinum nanoparticles on multilayered graphene petal nanosheets for electrochemical biosensing. Adv Func Mater 22(16):3399–3405. https://doi.org/10.1002/adfm.201200551

58. Su L, Feng J, Zhou X, Ren C, Li H, Chen X (2012) Colorimetric detection of urine glucose based $ZnFe_2O_4$ magnetic nanoparticles. Analy chem. 84(13):5753–5758

59. Zhu J et al (2021) Laser-induced graphene non-enzymatic glucose sensors for on-body measurements. Biosens Bioelectron. https://doi.org/10.1016/j.bios.2021.113606

Publisher's Note Springer Nature remains neutral with regard to jurisdictional claims in published maps and institutional affiliations.